Emergence of one- and two-cluster states in populations of globally pulse-coupled oscillators

Leonhard Lücken and Serhiy Yanchuk
Institute of Mathematics, Humboldt University of Berlin,
Unter den Linden 6, 10099 Berlin, Germany

February 22, 2011

1 Introduction

Networks of coupled dynamical systems play an important role for all branches of science [1, 2, 3, 4]. In the neuroscience, for instance, there is a need for modeling large populations of coupled neurons in order to approach problems connected with the synchronization of neural cells or other types of collective behavior [5, 6, 4]. The investigation of the dynamics of coupled lasers [7, 8, 9, 10] is important for many purposes including secure communication [11, 12] or high-power generation. The interacting biological, mechanical or electrical oscillators [13, 14] belong already to classical models for studying various aspects of collective dynamics. In neural networks, the synchronous activity might be pathological [15], and hence, there was recently an increasing effort to control the desynchronization of populations of coupled oscillators. In particular, the coordinated reset stimulation technique [4, 32] proposes to establish a cluster-state in the network, in which the oscillator's phases split into several subgroups. This example illustrates the importance of the analysis of cluster formation in coupled systems. Our paper investigates the connection between the properties of a single oscillator, i.e. its sensitivity to stimulations, and the formation of clusters in a globally coupled system of such oscillators. We show that by altering the shape of the sensitivity function, called the phase response function, different clusters in

a network can be stabilized. More presicely, we study a family of the phase response curves, which are unimodal and turn to zero at the spiking moment. This choice is motivated by several well known neuron models. It appears that the position of the maximum of the unimodal sensitivity function with respect to the spiking point plays an important role for determining whether the system will synchronize or approach a two-cluster state (see Fig 1). In particular, when the maximum of the sensitivity function is located in the second half of the period, the one-cluster (or completely synchronized) state acts as a global attractor. In the case, when the sensitivity function reaches its maximum in the first half of the period, various two-cluster states become stable.

1.1 Pulse-coupled oscillators

In some coupled systems, e.g. neuron populations, the time, during which the interaction effectively takes place is much smaller than the characteristic period of oscillations. In such cases, it is reasonable to approximate the interaction by an impact, i.e. by assuming that the interaction is immediate. This approximation leads to models of pulse-coupled oscillators, which have been widely used in the literature. For example, Mirollo and Strogatz [16] have shown, that the complete synchronization (in this case it is equivalent to the phase-locking) is stable and attracts almost all initial conditions in the network of globally coupled Integrate-and-Fire (IF) oscillators of the form

$$\frac{dx_j}{dt} = S_0 - \gamma x_j, \quad x_j \in [0,1), \quad j = 1, \ldots, N \tag{1}$$

with constants $S_0 > \gamma > 0$. One might refer to S_0 as input current and to γ as the dissipation constant. The following additional condition describes the interaction: when k-th oscillator reaches the threshold $x_k(t^-) = 1$, then positions of all remaining oscillators are shifted accordingly to the rule

$$x_j(t^+) = \min\{x_j(t) + \varkappa, 1\}, \quad j \neq k \tag{2}$$

with some small $\varkappa > 0$ and the k-th oscillator resets to $x_k(t^+) = 0$. It is shown in [16], that complete synchronization is achieved after a finite transient time. The synchronization in a more general model of IF neurons has been shown in [17]. Tsodyks *et al.* have demonstrated in [18] that the phase-locked state is unstable with respect to inhomogeneity in the local frequencies, i.e. when the oscillators become nonidentical.

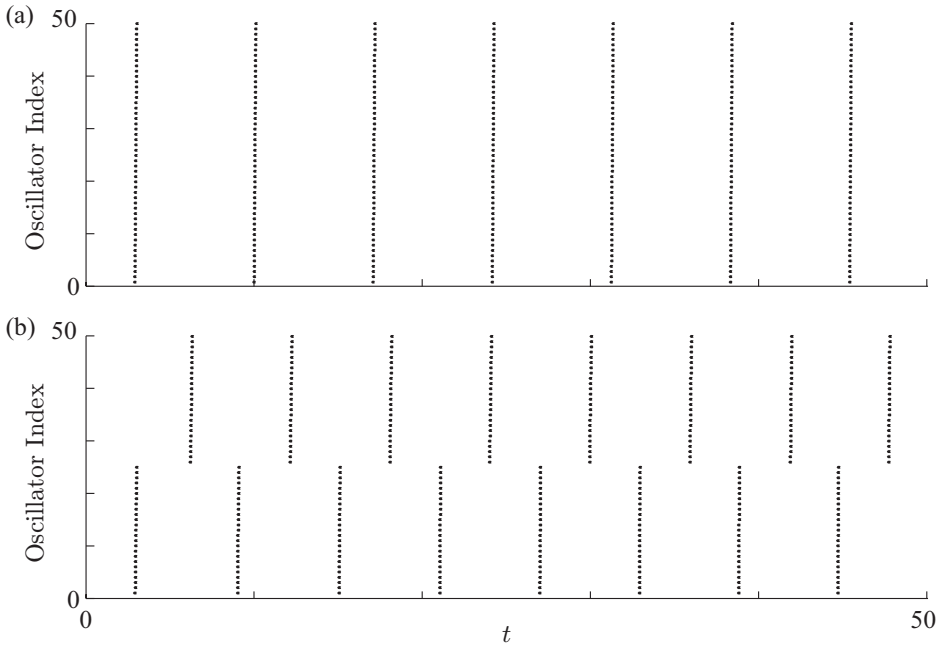

Figure 1: Clusters in a population of 50 phase-oscillators. Dots indicate the times when an oscillator reaches the threshold; (a) shows the firing pattern of a complete in-phase synchronized population (one-cluster), while (b) shows the firings in a symmetric two-cluster.

A larger class of pulse-coupled models was studied in [19, 20, 21]. In particular, Goel and Ermentrout [19] obtained sufficient conditions for the stability of a completely synchronous solution. We introduce this class of models in the subsection 1.2.

The dynamics of pulse-coupled oscillators has been studied also for systems with different topologies, i.e. ring topology [22], as well as for delayed interactions [23]. Transient phenomena of randomly diluted networks have been analyzed in [24]. Globally pulse-coupled IF oscillators with a finite pulse-width have been considered in, e.g. [25, 26, 27], where the interaction pulse is assumed to have a shape $\frac{\alpha^2 t}{N} e^{-\alpha t}$ with the width α.

1.2 Phase-response curve as a parameter

In this subsection we introduce a general class of pulse-coupled phase oscillators [19, 28]. The oscillator's motion between the spikes is described by the

rule

$$\frac{d\varphi_j}{dt} = \omega, \tag{3}$$

where $\varphi_j \in [0, 2\pi]$. When k-th oscillator reaches the threshold at time t, i. e. $\varphi_k(t^-) = 2\pi$, it emits a spike to all other oscillators of the network, which are immediately resetted according to

$$\varphi_k(t^+) = 0; \quad \varphi_j(t^+) = \varphi_j(t^-) + \varkappa Z(\varphi_j(t^-)), \quad j \neq k, \tag{4}$$

where $Z(\varphi)$ is called *phase response curve* (PRC). Effectively, this means that there is no coupling between two consecutive spiking events. The coupling occurs only during the spike and acts through the resetting, since the time of the resetting of the oscillator j depends on the phase position of the oscillator k. The size of the phase-jump, that an oscillator performs, when stimulated by an incoming spike depends on its sensitivity to stimulation in its present state. See figure 2 for an illustration.

Let us firstly show, that IF oscillators (1) can be written in a form similar to (3)–(4), see also [19]. For this, we rewrite (1) with respect to the phase coordinate instead of the voltage coordinate. Indeed, the coordinate x_j in system (1) is supposed to describe the voltage difference across the membrane of a neuron [29]. The phase coordinate φ_j should behave accordingly to (3) with the frequency $\omega = 2\pi/T$, where T is the period of oscillations without interaction and can be found from (1)

$$T = -\frac{1}{\gamma} \ln\left(1 - \frac{\gamma}{S_0}\right).$$

The corresponding transformation of variables $x = f(\varphi)$ can be found from the condition

$$\frac{dx}{dt} = \frac{df}{d\varphi}\frac{d\varphi}{dt} = \frac{df}{d\varphi}\omega = S_0 - \gamma f(\varphi),$$

i.e. from the initial value problem

$$\frac{df(\varphi)}{d\varphi} = \frac{T}{2\pi}(S_0 - \gamma f(\varphi)), \quad f(0) = 0. \tag{5}$$

This gives the function

$$f(\varphi) = \frac{S_0}{\gamma}\left(1 - \exp\left(-\frac{\gamma T}{2\pi}\varphi\right)\right),$$

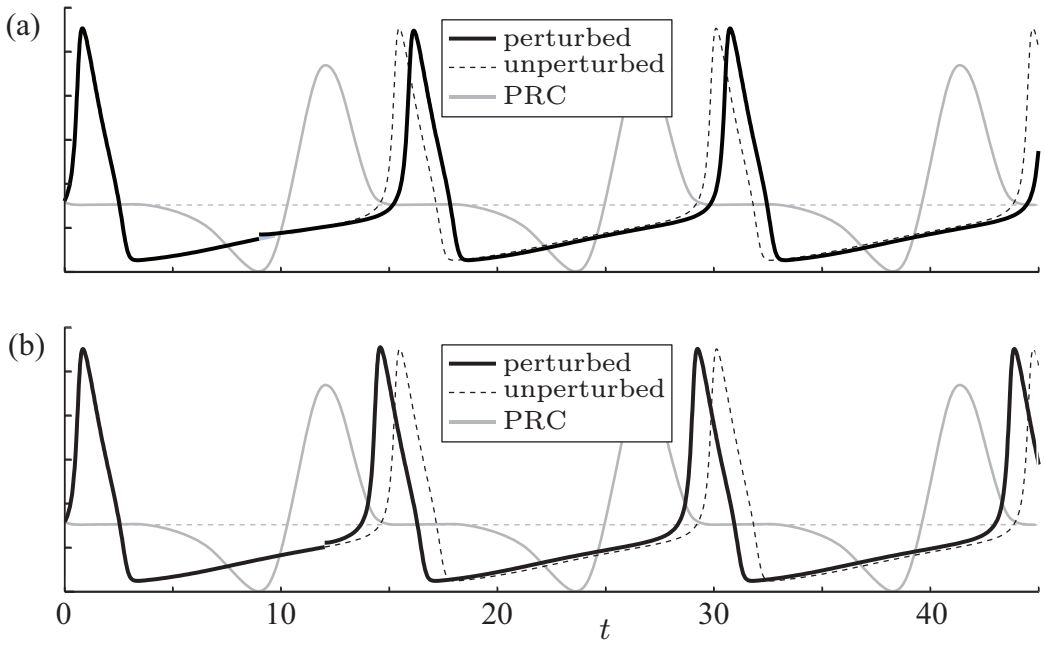

Figure 2: Periodic spiking in a Hodgkin-Huxley neuron model. Solid black lines show the evolution of the voltage-component of the model when perturbed by a weak pulse at $t = 9$ in (a), resp. $t = 12$ in (b). The dashed black lines show the unperturbed oscillations. The PRC $Z(\varphi(t))$ of the unperturbed model is plotted solid grey and the dashed grey line corresponds to $Z = 0$. The outcome of the perturbing pulse depends on the time t, or equivalently on the phase $\varphi(t)$, of its application. Either, the phase is delayed as in (a), i. e. $Z(\varphi(t)) < 0$, or it is forwarded as in (b), i. e. $Z(\varphi(t)) > 0$.

which maps the interval $0 \leq \varphi \leq 2\pi$ into $0 \leq x \leq 1$. In the transformed coordinates φ_j, the dynamics between the spikes is described by (3). It remains to specify the dynamics at the threshold. Taking into account (2), when k-th oscillator reaches the threshold $\varphi_k(t^-) = 2\pi$ its phase φ_k resets to $\varphi_k(t^+) = 0$ and all other oscillators have the impact

$$\begin{aligned} \varphi_j(t^+) = f^{-1}\left(x_j(t^+)\right) &= f^{-1}\left(x_j(t) + \varkappa\Delta(\varkappa, x_j(t))\right) \\ &= f^{-1}\left(f(\varphi_j(t)) + \varkappa\Delta(\varkappa, f(\varphi_j(t)))\right), \end{aligned}$$

where $\Delta(\varkappa, x) = \min\{1, (1-x)/\varkappa\} \leq 1$. In the case of small $\varkappa$, i.e. the assumption of weak coupling holds, the resetting rule can be approximated

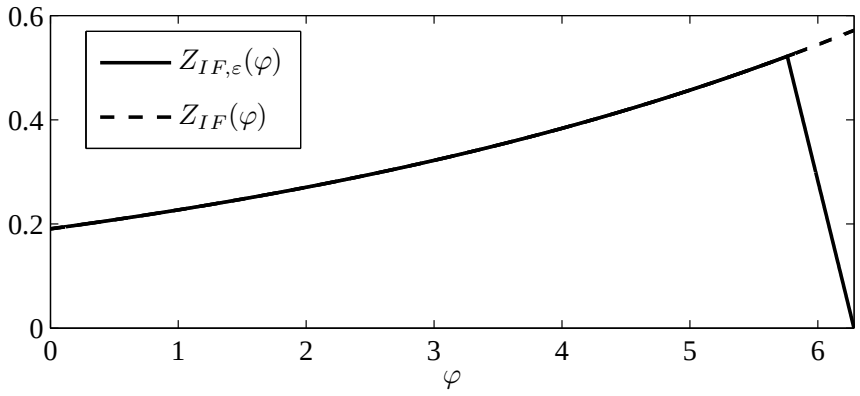

Figure 3: Phase-response curve for IF model (1). The function $Z_{IF}(\varphi)$ measures the sensitivity of the system to a small external perturbation at different positions φ. The corrected function $Z_{IF,\varkappa}(\varphi)$ does not allow the oscillators to be moved over the threshold by a spike.

as

$$\varphi_j(t^+) = \varphi_j(t) + \varkappa \min\{Z_{IF}(\varphi_j(t)), (2\pi - \varphi_j(t))/\varkappa\}, \tag{6}$$

where

$$Z_{IF}(\varphi) := \frac{d(f^{-1})}{dx}(f(\varphi)) = \frac{2\pi T}{S_0} \exp\left(\frac{T\gamma}{2\pi}\varphi\right). \tag{7}$$

Thus, with respect to the phase coordinates, the IF model (1) has the form (3), (6). In particular, the resetting rule is given by the function

$$Z_{IF,\varkappa}(\varphi) = \min\{Z_{IF}(\varphi_j(t)), (2\pi - \varphi_j(t))/\varkappa\}, \tag{8}$$

which depends on the amplitude of the perturbation $\varkappa$. Figure 3 illustrates this function for $\varkappa = 0.05$. Practically, the PRC measures the sensitivity of the phase to external perturbations.

We have shown above the specific example of pulse-coupled IF models and their reduction to pulse-coupled phase oscillators (3)–(4). In fact, this procedure is also possible for higher-dimensional smooth systems, whenever the oscillations correspond to a hyperbolic limit cycle, i.e. in a generic case. More details can be found in [19, 28, 30]. When the coupling is acting along one component, e.g. the voltage variable, as often assumed in the case of neural populations, the PRC appears as a scalar function of the phase. In

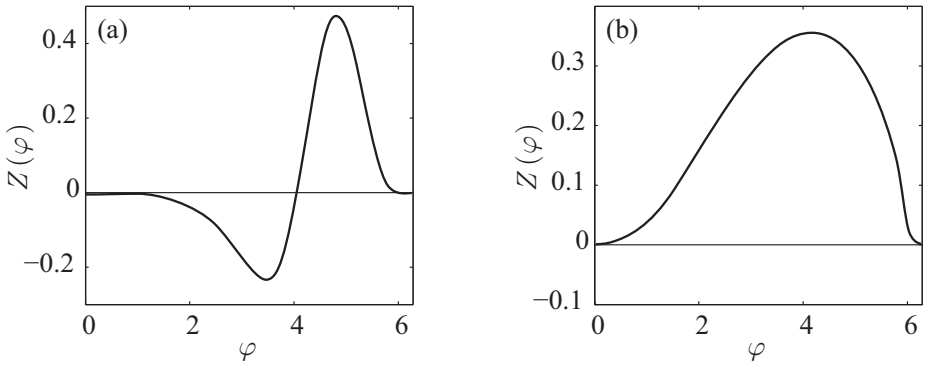

Figure 4: Examples of different PRCs. (a) Hodgkin-Huxley model, (b) Connor model. Note that the functions and their derivatives are zero at the ends of the interval $\varphi = 0$ and $\varphi = 2\pi$ (adapted from [31]).

the case of a higher-dimensional interaction, it should be considered more generally as a vector.

Examples of PRCs for different neuron models are shown in Fig. 4. Some more numerically and experimentally obtained PRCs can be found in e.g. [19, 28, 31]. The remarkable feature of many of such PRCs is that, contrary to the IF model, their PRCs are independent on $\varkappa$ and admit zero values at $\varphi = 0$ and $\varphi = 2\pi$. The conditions $Z(0) = Z(2\pi) = 0$ are also reasonable from the neuroscientific point of view, since they reflect the fact that the neurons are not sensitive to perturbations during the spike (see Fig. 4). Generally speaking, system (3)–(4) is a useful model, which possesses quite a big generality by including the PRC as some "infinite-dimensional" parameter.

1.3 System description

Our main object of study is the following system of globally pulse-coupled phase oscillators of the form

$$\frac{d\varphi_j}{dt} = 1 \tag{9}$$

with the resetting rule

$$\varphi_k(t^+) = 0; \quad \varphi_j(t^+) = \varphi_j(t^-) + \frac{\varkappa}{N} Z(\varphi_j(t^-)), \quad j \neq k, \tag{10}$$

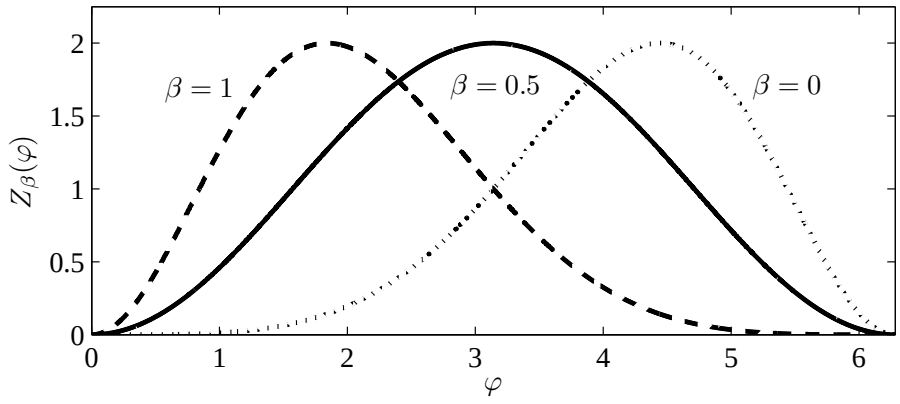

Figure 5: Family of the unimodal PRCs $Z_\beta(\varphi)$, see (11).

where the velocity of the phase is assumed to be 1 without loss of generality. We assume a fixed, positive overall coupling strength $\varkappa > 0$. The impact is rescaled taking into account the number of oscillators, see also [27]. In this study, we consider a one-parametric family of the PRCs, which are positive and unimodal as shown in Fig. 5. The parameter $\beta \in [0, 1]$ controls the position of the maximum, namely, for larger β, the maximum is located in the domain of small φ, which corresponds to a more sensitive excitatory response of the system just after spike. For smaller β, the system is more sensitive to perturbations shortly before the spike. The value $\beta = 0.5$ corresponds to an intermediate situation. We assume also that $Z'(0) = Z'(2\pi) = 0$, which is appropriate for a broad class of experimental and analytically obtained PRCs (see Fig. 4).

We note that the qualitative results reported in the paper are independent on the exact expression for the PRC but rather on the shape of the PRC and its behavior at $\varphi = 0$ and $\varphi = 2\pi$. Our particular choice is

$$Z_\beta(\varphi) = 1 - \cos \vartheta_\beta(\varphi), \quad \beta \in [0, 1]\,, \tag{11}$$

where

$$\vartheta_\beta(\varphi) = (1 - \beta)\,\frac{\varphi^2}{2\pi} + \beta \left(2\pi - \frac{(\varphi - 2\pi)^2}{2\pi} \right).$$

In particular, $Z_{0.5}(\varphi) = 1 - \cos \varphi$.

System (9)–(10) is equivalent to an $(N-1)$-dimensional discrete dynamical system, which can be obtained as a return map by considering its state

each time when some of the phases reaches a fixed value, e.g. $\varphi_1 = 2\pi$. Let us point out how this map appears. Without loss of generality, we may assume that the phases are ordered as

$$2\pi = \varphi_1 \geq \varphi_2 \geq \cdots \geq \varphi_N \tag{12}$$

at $t = 0$. We will use the important property of (9)–(10) that the oscillators do not overrun each other for all times if the system size N is sufficiently large. Indeed, since the inequality

$$\varphi_j + \frac{\varkappa}{N} Z(\varphi_j) \geq \varphi_{j+1} + \frac{\varkappa}{N} Z(\varphi_{j+1}) \tag{13}$$

holds for sufficiently large N, the order of oscillators is preserved during the spike. It is also evident, that the order is preserved between the spikes as well. More exactly, the inequality $2\pi \geq \varphi_{1+l} \geq \varphi_{2+l} \geq \cdots \geq \varphi_{N+l} \geq 0$ holds for all t, where l is some shift and the indices are considered modulo N.

Let us denote by K_1 the map, which maps the initial phases (12) into the phases at the moment when the oscillator φ_2 reaches the threshold, i.e. $\varphi_2 = 2\pi$. It is easy to obtain that

$$\begin{aligned} &K_1(\varphi_1, \varphi_2, \varphi_3, \ldots, \varphi_N) = \\ &= (2\pi - \mu(\varphi_2), 2\pi, \mu(\varphi_3) + 2\pi - \mu(\varphi_2), \ldots, \mu(\varphi_N) + 2\pi - \mu(\varphi_2)), \end{aligned}$$

where

$$\mu(\varphi) := \varphi + \frac{\varkappa}{N} Z(\varphi). \tag{14}$$

In a similar way, the mapping K_2 exists, which maps the phases to the state, where the third oscillator is at the threshold and so on. The composition of maps

$$K = K_N \circ K_{N-1} \circ \cdots \circ K_1 \tag{15}$$

gives the dynamical system on N-dimensional torus $\mathbb{T}^N$

$$(\varphi_1, \ldots, \varphi_N) \to K(\varphi_1, \ldots, \varphi_N), \tag{16}$$

which maps the initial state (12) into a new state after all N oscillators have crossed the threshold once and the first oscillator reaches again the threshold. We call the map K *return map*.

In this paper, we will not use the explicit form of the mapping (15). For our purposes it is important to conclude that the dynamics of system (9)–(10) are indeed equivalent to some $(N-1)$-dimensional, discrete dynamical system on the N-dimensional torus. The smoothness of this system depends on the smoothness of its PRC function.

2 Numerical results

In order to detect the appearance of one- or two-cluster states, we have numerically computed the order parameters

$$R_1(t) = \left| \frac{1}{N} \sum_{k=1}^{N} e^{i\varphi_k(t)} \right| \tag{17}$$

and

$$R_2(t) = \left| \frac{1}{N} \sum_{k=1}^{N} e^{i2\varphi_k(t)} \right|. \tag{18}$$

A perfect one-cluster state is characterized by $R_1 = R_2 = 1$ and a perfect antiphase two-cluster is characterized by $R_1 = 0$ and $R_2 = 1$. We present results of simulations for $\varkappa = 0.5$, but qualitatively we observe similar behavior for a broad range of $\varkappa > 0$.

As shown in Fig. 6, we observe two qualitatively different types of behavior depending on parameter β. For $\beta < 0.5$, i.e. when the maximum of the PRC is shifted to the right (see Fig. 5), the one-cluster state seems to be the attractor; for $\beta > 0.5$ and the maximum of the PRC is shifted to the left, a two-cluster state is attracting. We have chosen initial conditions in a vicinity of a two-cluster state in Fig. 6(a) and (b), therefore the initial values of the order parameters are $R_1 \approx 0$ and $R_2 \approx 1$. Figure 6(b) shows how the instability of the two-cluster state implies desynchronization transient, after which the system is attracted to a synchronous one-cluster state. Similar behavior occurs for other initial conditions. Figure 6(c) and (d) illustrate the order parameters behavior for initial conditions close to the splay state (a state, where the phases are distributed). The initial values for the order parameters in the splay state are close to zero, but after a transient, they approach again the same asymptotic values as in (a) and (b).

A more complicated behavior occurs for the intermediate value of the parameter $\beta = 0.5$, i.e. when the PRC is symmetric. In this case, the order

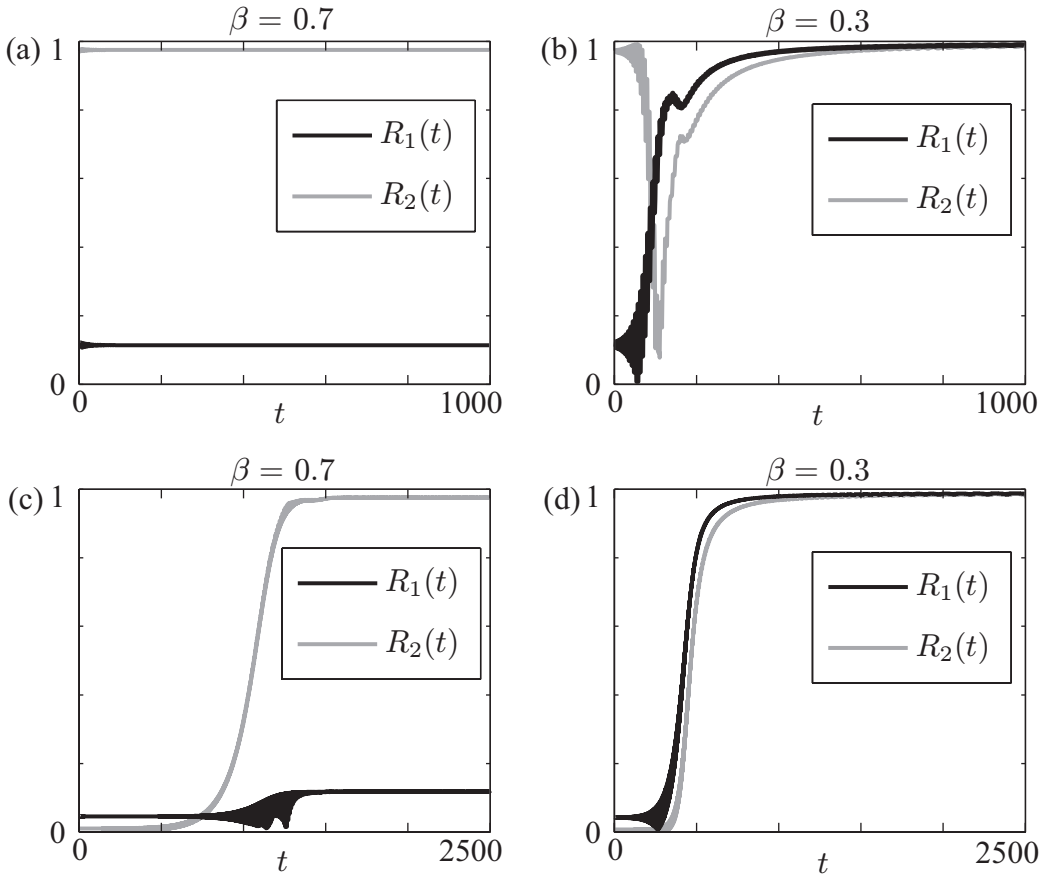

Figure 6: Behavior of the order parameters $R_1(t)$ and $R_2(t)$ for a trajectory starting in a vicinity of the two-cluster state for (a) and (b). The lower panel (c) and (d) corresponds to a trajectory starting in a vicinity of the splay state. Left figures (a) and (c) correspond to the parameter value $\beta = 0.7$, where the two-cluster state is attracting and (b) and (d) to $\beta = 0.3$, where one-cluster state is attracting.

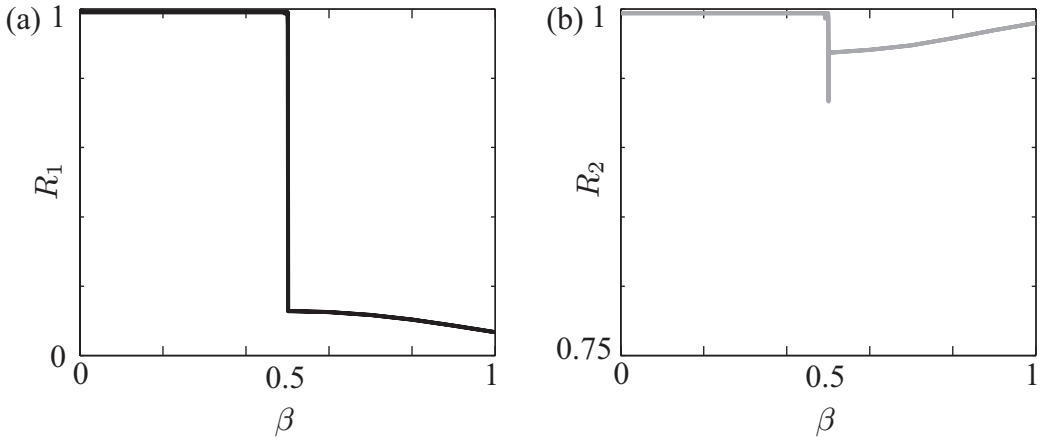

Figure 7: Dependence of the asymptotic values for the order parameter R_1 (a) and R_2 (b) on β. For the most values of β, except $\beta = 0.5$, the order parameters tend to some constant value, when initialized near the splay state or the symmetric two-cluster state.

parameters $R_1(t)$ and $R_2(t)$ do not approach some asymptotic constant values but remain periodic in time. As a result, the maximum asymptotic values of both R_1 and R_2 do not coincide with the corresponding minimum values. This type of behavior is observed for a very small parameter interval of order 10^{-3} around $\beta = 0.5$. We discuss it in Sec. 5 in more details. Figure 7 summarizes the behavior of the order parameters for different β.

3 Appearance and stability properties of one-cluster state

In an ideal one-cluster synchronized state, all oscillators have the same phases $\varphi_j = \varphi_s$ for all j. This state is a fixed point of the map (16), because the PRC turns to zero at $\varphi = 2\pi$ and $\varphi = 0$. This means that the coupling vanishes for one-cluster state. More exactly, when an oscillator φ_j fires, i.e. $\varphi_j = 2\pi$, all other oscillators have the phase 2π and do not obtain the spike. As a result, the period of this state is determined simply by the uncoupled dynamics and equals 2π.

3.1 Inadequacy of the linear stability analysis

In order to obtain conditions for the stability of one-cluster state, one can examine the return map (16). The linearization of this return map around the one-cluster state gives then the corresponding multipliers, which determine its local linear stability. As it is expected, the local stability is governed by the properties of the PRC at $\varphi = 0$ and $\varphi = 2\pi$. This procedure has been done in [19]. Applying these results to our case, the resulting conditions for the local linear stability of one-cluster state is

$$\left(1 + \frac{\varkappa}{N} Z'(2\pi^-)\right)^l \left(1 + \frac{\varkappa}{N} Z'(0^+)\right)^{N-l} < 1, \quad l = 1, N-1. \tag{19}$$

We observe that the necessary condition for the linear stability is that the derivatives of $Z(\varphi)$ at the ends of the interval $[0, 2\pi]$ do not vanish. This is not the case for our PRC (11). Hence, all associated multipliers have modulus one and the linear stability analysis do not provide useful information about the stability of one-cluster state.

3.2 One-cluster state is a saddle point

In this section we show that one-cluster state is a saddle point, i.e. there are some arbitrary small perturbations of this state, which grow with time. At the same time, some other small perturbations decay.

Existence of a local unstable direction. First of all, let us show that one-cluster state is unstable with respect to the following special perturbation:

$$\varphi_1 = \varphi_s + \varepsilon, \quad \varphi_2 = \cdots = \varphi_N = \varphi_s \tag{20}$$

with arbitrary small $\varepsilon > 0$. During the period between spikes, the dynamics is monotonous $\varphi_j(t) = \varphi_s + t$ for $j = 2, \ldots, N$ and $\varphi_1(t) = \varphi_s + \varepsilon + t$, thus, the distance between the phases remain constant. Without loss of generality we may assume that

$$\varphi_1(0^-) = 2\pi, \quad \varphi_2(0^-) = \cdots = \varphi_N(0^-) = 2\pi - \varepsilon.$$

After the first oscillator moves over the threshold and resetting occurs, the phases are as follows

$$\varphi_1(0^+) = 0, \quad \varphi_2(0^+) = \cdots = \varphi_N(0^+) = 2\pi - \varepsilon + \frac{\varkappa}{N} Z(2\pi - \varepsilon) = \mu(2\pi - \varepsilon).$$

The next resetting occurs at time $t_1 = 2\pi - \varphi_2(0^+) = \varepsilon - \frac{\varkappa}{N} Z(2\pi - \varepsilon)$ when the group of $N-1$ synchronous oscillators reaches the threshold. At this moment

$$\varphi_1(t_1^-) = \varepsilon - \frac{\varkappa}{N} Z(2\pi - \varepsilon) > 0, \quad \varphi_2(t_1^-) = \cdots = \varphi_N(t_1^-) = 2\pi.$$

Now the group of $N-1$ synchronous oscillators is at the threshold. The correct definition of the firing rule for this case can be naturally obtained by extending it to the situation when all the oscillators $\varphi_2, \ldots, \varphi_N$ in the cluster have slightly different phases and then allowing the phases to converge to the same value. This leads to the following resetting rule when passing the threshold by the $N-1$ cluster:

$$\varphi_1(t_1^+) = \mu^{N-1}\left(\varphi_1(t_1^-)\right) = \mu^{N-1}\left(\varepsilon - \frac{\varkappa}{N} Z(2\pi - \varepsilon)\right), \tag{21}$$

$$\varphi_2(t_1^+) = \cdots = \varphi_N(t_1^+) = 0, \tag{22}$$

where μ^{N-1} denotes the superposition of $N-1$ functions $\mu \circ \mu \circ \mu \circ \cdots \circ \mu$, where μ is defined by (14). The resetting (21) simply means that the function μ is applied $N-1$ times (whenever an oscillator from the cluster $\varphi_2, \ldots, \varphi_N$ fires) in order to obtain the final position of φ_1.

In this way, we obtain a mapping, which maps the initial size of the perturbation ε at time $t = 0$ into its new size $Y_1(\varepsilon)$ at time t_1. The mapping is

$$\varepsilon \to Y_1(\varepsilon) = \mu^{N-1}\left(\varepsilon - \frac{\varkappa}{N} Z(2\pi - \varepsilon)\right). \tag{23}$$

It is clear that $Y_1(0) = 0$, what corresponds to the invariance of the one-cluster, and the stability properties of the origin of (23) determine the stability of the one-cluster state with respect to the specific perturbation (20) chosen. Up to the linear level, the origin of (23) is neutrally stable, i.e. $Y_1'(0) = 1$, which is clear, since the one-cluster state is linearly neutrally stable. The second derivative of (23) at $\varepsilon = 0$ is nontrivial

$$Y_1''(0) = \varkappa Z''(0) - \frac{\varkappa}{N}\left(Z''(2\pi) + Z''(0)\right)$$

and is positive for sufficiently large N since $Z''(0) > 0$ for $\beta \in (0, 1]$. Hence, for sufficiently large N, the origin of (23) is unstable, see Fig. 8(a). *This leads to the local instability of one-cluster state for all* $\beta \in (0, 1]$. Accordingly to this, the distance of the advanced oscillator φ_1 from the remaining cluster will grow, but this growth is not exponential.

Existence of a local stable direction. Now let us show that the one-cluster state is locally stable with respect to perturbations of the form

$$\varphi_1 = \varphi_s - \varepsilon, \quad \varphi_2 = \cdots = \varphi_N = \varphi_s \tag{24}$$

with $\varepsilon > 0$. This can be shown similarly to the previous case by obtaining the discrete mapping, which describes the dynamics of the perturbation. In the case of perturbations (24), this mapping reads

$$\varepsilon \to Y_{N-1}(\varepsilon) = \mu\left(2\pi - \mu^{N-1}(2\pi - \varepsilon)\right) \tag{25}$$

and has the following properties

$$Y_{N-1}(0) = 0,$$

$$Y'_{N-1}(0) = 1,$$

and

$$Y''_{N-1}(0) = -\varkappa Z''(2\pi) + \frac{\varkappa}{N}\left(Z''(2\pi) + Z''(0)\right) \tag{26}$$

It implies that for sufficiently large N the second derivative is negative and the origin of the discrete mapping $\varepsilon \to Y_{N-1}(\varepsilon)$ is asymptotically stable (see Fig. 8(b)). Hence, the one-cluster state is stable with respect to perturbations of the form (24). This, together with the instability with respect to perturbations (20), implies that the one-cluster state is the saddle point in the phase space (see schematically Fig. 9).

Other stable and unstable local directions. In general, the two-cluster perturbations of the one-cluster state are given by

$$\varphi_1(0) = ... = \varphi_{N_1}(0) = 2\pi \tag{27}$$

$$\varphi_{N_1+1}(0) = ... = \varphi_N(0) = 2\pi - \varepsilon, \tag{28}$$

where $N_1 + N_2 = N$. This means, there are N_1 oscillators in the front-group and the remaining N_2 oscillators in the back-group. The corresponding discrete 1-D systems, which describe the dynamics of such perturbations are given by

$$\varepsilon \to Y_{N_1}(\varepsilon) \text{ and } \varepsilon \to Y_{N_2}(\varepsilon),$$

where $Y_j(0) = 0$, $\frac{d}{d\varepsilon}Y_j(0) = 1$ for $j = 1, ..., N-1$ and

$$\frac{d^2}{d\varepsilon^2}Y_{N_1}(0) = \frac{\varkappa}{N}\left(N_2 Z''(0) - N_1 Z''(2\pi)\right), \tag{29}$$

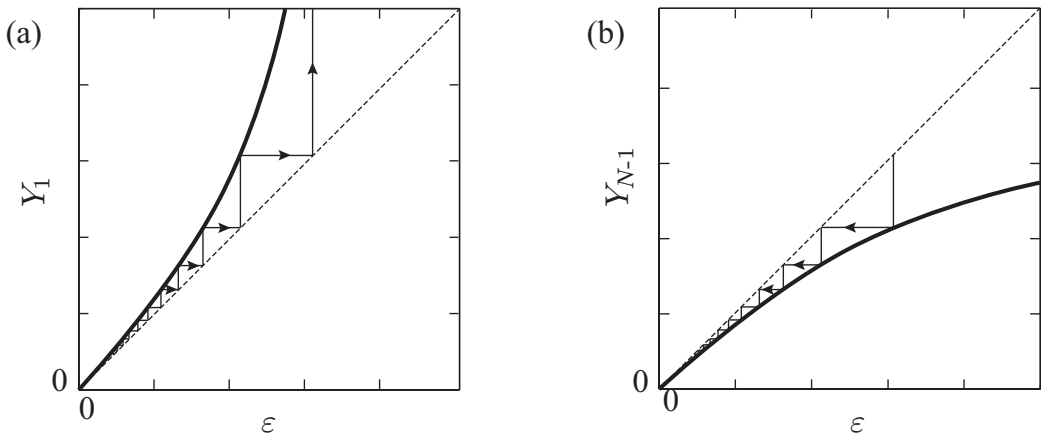

Figure 8: Local Cobweb-Diagram of the functions $Y_1(\varepsilon)$ and $Y_{N-1}(\varepsilon)$ around $\varepsilon = 0$. Iterations of these maps determine the behavior of special perturbations to the one-cluster state. (a): small perturbations grow with time; (b): small perturbations decay.

$$\frac{d^2}{d\varepsilon^2} Y_{N_2}(0) = \frac{\varkappa}{N} \left(N_1 Z''(0) - N_2 Z''(2\pi) \right). \tag{30}$$

The expressions (29) and (30) may have different signs depending on the values of N_1, N_2, as well as the second derivatives $Z''(0)$ and $Z''(2\pi)$. This implies the existence of multiple unstable as well as stable directions to the one-cluster solution, for more details, see section 4.

3.3 Stable homoclinic orbit to one-cluster state

Let us first note that the two-clusters of the form (27)–(28) do not split with time. In geometric terms, this means, that the subspace corresponding to such solutions is invariant. In particular, the subspace, which corresponds to $N_1 = 1$ and $N_2 = N-1$ is invariant as well. Being restricted to this invariant subspace, the one-cluster state is a saddle point, as we have shown in the previous section. In Appendix 7 we prove that there exists a homoclinic orbit in this subspace, which connects the both unstable and stable manifolds, see Fig. 9. In fact, as will be shown in Sec. 4, the dynamics within the invariant subspace is given by the 1-D mapping shown in Fig. 11(b).

Numerical calculations further supports this result and show that the invariant set, which is composed of a homoclinic loop and the fixed point is

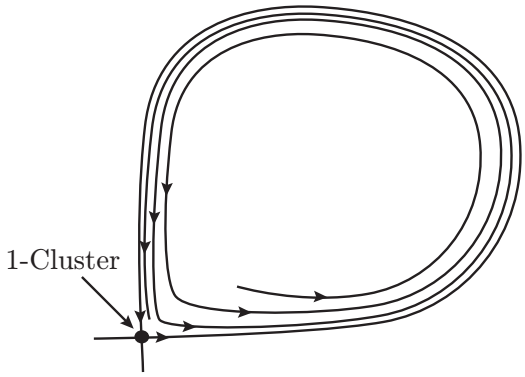

Figure 9: One-cluster state as a saddle point in the phase space with a homoclinic loop.

an attractor. Figure 10 shows how the width of the cluster changes as time evolves for some typical initial conditions. More specifically, we compute

$$\Delta(t) = \max_{1\le i,j\le N} \{|\varphi_i(t) - \varphi_j(t)|\}\,.$$

One can clearly observe that the width tends eventually to zero interrupted by some blowouts. The blowouts correspond to the events, during which the first oscillator leaves behind the remaining cluster and makes a rotation in the phase. After the rotation, it joins again the cluster and becomes the "last" one. The time interval between such events grows unboundedly with time supporting the homoclinic nature of the attractor. Note that the width of the cluster should be nonzero in order to observe this phenomenon, i.e. one should perturb the system slightly from the fixed point, see Fig. 9.

Finally, we would like to remark that the same methods allow proving the existence of other homoclinic orbits, which correspond to two-cluster perturbations (27)–(28) with $N_1 \ll N_2$. Hence, one should rather speak about an attracting family of homoclinic orbits.

4 Two-cluster states

Two-cluster state appears when the oscillators split into two groups (see Fig. 1)

$$\varphi_1 = \cdots = \varphi_{N_1} := \psi_1, \quad \varphi_{N_1+1} = \cdots = \varphi_{N_1+N_2} := \psi_2. \tag{31}$$

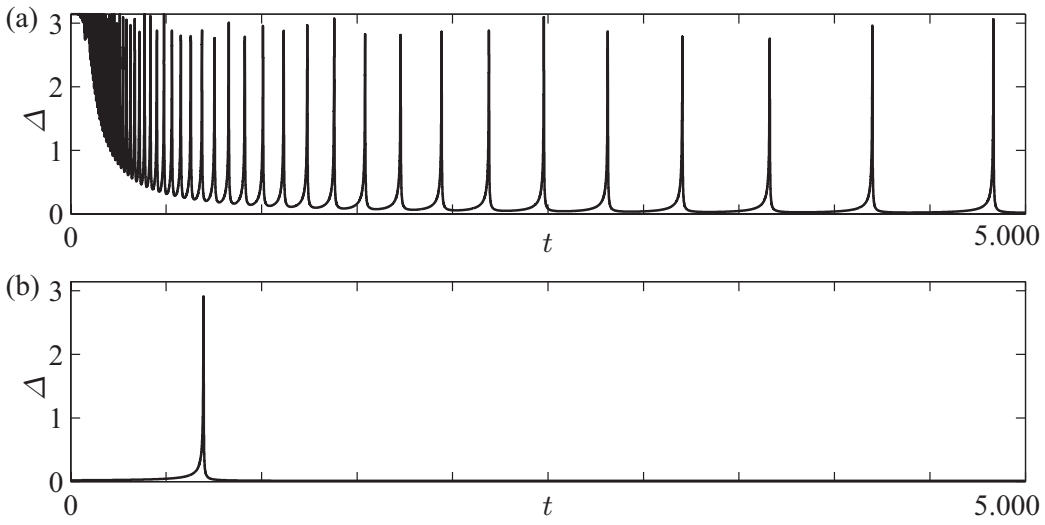

Figure 10: Width of the cluster $\Delta(t) = \max_{1\leq i,j\leq N}\{|\varphi_i(t) - \varphi_j(t)|\}$ as a function of time. Figure (a) shows the behavior along the orbit started at an initial condition close to the splay state (far from the one-cluster). (b) shows the behavior along the orbit started close to the state (20). The behavior indicates the existence of a stable homoclinic orbit.

Contrary to one-cluster state, the two-cluster state must not be a fixed point of the return map (16). Indeed, when two clusters appear, their relative behavior is then given by the following discrete return map (by assuming that the return map is computed for $\psi_1 = 2\pi$ and $\psi_2 < \psi_1$)

$$\psi_2 \to Y_{N_1}(\psi_2) := 2\pi - \mu^{N_2}\left(2\pi - \mu^{N_1}(\psi_2)\right). \tag{32}$$

This map has different properties depending on N_1, $N_2 = N - N_1$ as well as on β. All such maps have zero fixed point corresponding to the case when two clusters merge into one. One can obtain

$$Y_{N_1}(0) = 0, \quad Y_{N_1}(2\pi) = 2\pi,$$

$$Y'_{N_1}(0) = 1, \quad Y'_{N_1}(2\pi) = 1,$$

and

$$Y''_{N_1}(0) = \frac{\varkappa}{N}\left(N_2 Z''(0) - N_1 Z''(2\pi)\right),$$

$$Y''_{N_1}(2\pi) = \frac{\varkappa}{N}\left(N_2 Z''(2\pi) - N_1 Z''(0)\right).$$

Figure 11 shows typical maps for three different situations:
(a) The map has an unstable fixed point inside the interval $[0, 2\pi]$ and the endpoints $x = 0$ and $x = 2\pi$ are asymptotically stable. Hence, within the corresponding subspace, the one-cluster state is asymptotically stable (similarly to Fig. 8(b)).
(b) The map has unstable fixed point at $x = 0$ and stable at $x = 2\pi$. This case corresponds exactly to the case, when the one-cluster state has a homoclinic orbit starting in $x = 0$ and ending at $x = 2\pi$ ($0 \sim 2\pi$ on the torus).
(c) The map has a stable fixed point inside the interval $[0, 2\pi]$ and the endpoints $x = 0$ and $x = 2\pi$ are unstable. Hence, within the corresponding subspace, the one-cluster state is asymptotically unstable and the two-cluster stationary state is stable.

The fixed points of the map (32) give two-cluster stationary states:

$$\psi_2 = Y_{N_1}(\psi_2). \tag{33}$$

The condition for the merging of two cluster into one cluster is given by the condition for the existence of the double root of the function $Y_{N_1}(\psi)$ at $\psi = 0$ or $\psi = 2\pi$, i.e. $Y''_{N_1}(0) = 0$ or $Y''_{N_1}(2\pi) = 0$. This results into

$$N_1 Z''(0) = N_2 Z''(2\pi). \tag{34}$$

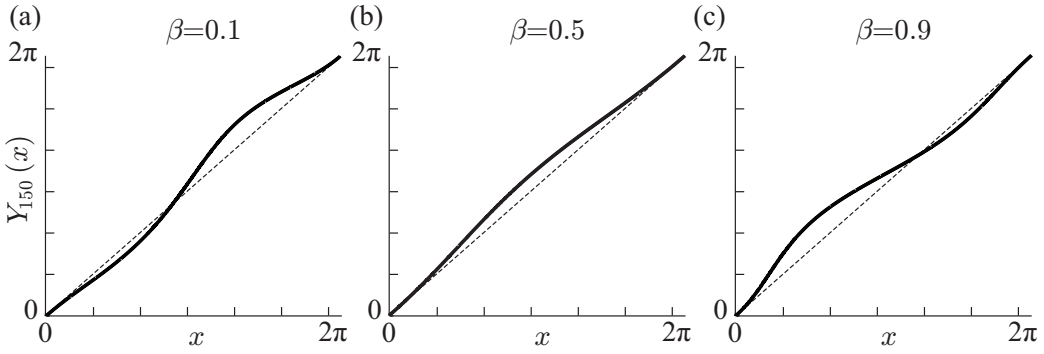

Figure 11: Typical behavior of functions $Y_{N_1}(x)$ (see (32)), which determine the behavior of two-clusters. On the figure $N_1 = 150$ and $N = 500$.

Expression (34) determines also the moments when one-cluster state undergoes pitchfork bifurcations. At such bifurcation, two different nonsymmetric two-clusters bifurcate from the one-cluster state: one with $N_1 = pN$, $N_2 = (1-p)N$, and another with $N_1 = (1-p)N$, $N_2 = pN$. The bifurcation diagram in Fig. 12 shows some of the branches of two-clusters, which originate from $\psi_2 = 0$ or $\psi_2 = 2\pi$.

The pitchfork bifurcations for $\beta < 0.5$ are subcritical. Namely, the two-cluster states are unstable and they merge into the one-cluster state. With increasing β the one-cluster state becomes more and more locally unstable by transforming stable directions into homoclinics (see Fig.11). In spite of this fact, we observe numerically, that the invariant set, which is composed of the one-cluster state and homoclinic connections is still attracting in the phase space. All two-cluster states, which exist at this moment, are unstable. As a result, one computes high values of the order parameters R_1 and R_2 on the numerically obtained figure 7 for $\beta < 0.5$.

4.1 Stability of two-cluster states

For $\beta > 0.5$, the invariant set composed of one-cluster state and homoclinic orbits losses its stability and two-cluster states emerge, which are asymptotically stable. Numerical results in Fig. 13 show which two-clusters are stable depending on the parameter β. In general, for β closer to 0.5, the symmetric clusters with $p \approx 0.5$ are stable. As β increases, the more asymmetric clusters stabilize as well. This implies that the PRCs with the maximum,

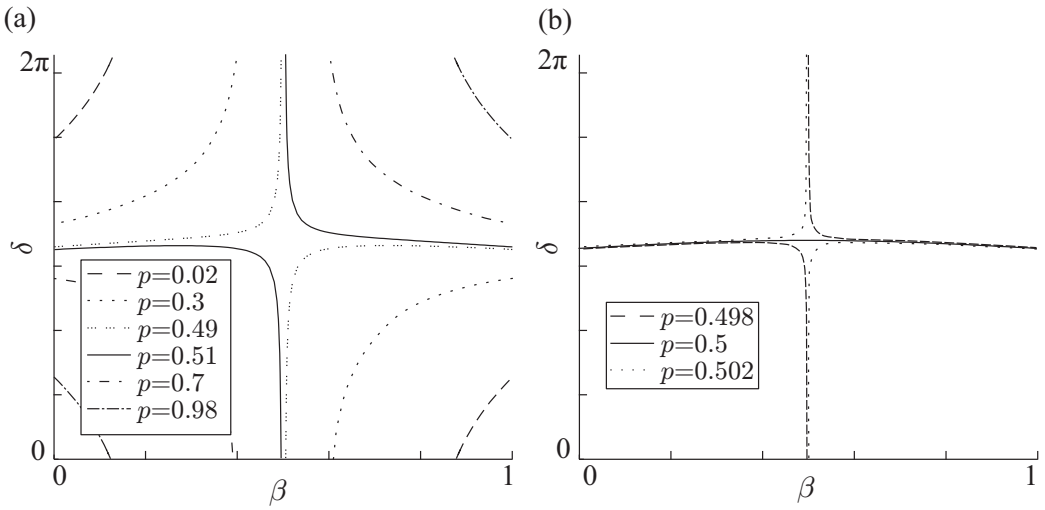

Figure 12: Positions of the two-cluster states $\delta = 2\pi - \psi_2$, where ψ_2 are fixed points of (33). Different lines correspond to different cluster splittings, i.e. $N_1 = pN$, $N_2 = (1-p)N$. At $\delta = 0$ or $\delta = 2\pi$, the corresponding two-cluster is merging into the one-cluster.

which is shifted to the left favor the coexistence of a large number of stable branches of two-clusters.

5 Intermediate state for symmetric PRC with $\beta = 0.5$

The case of symmetric PRC for $\beta = 0.5$ is degenerate. When increasing β through 0.5, the homoclinic sets including the one-cluster state become unstable and a two-cluster state becomes stable as it is described in the previous section. The numerical calculations for $\beta = 0.5$ show nonstationary dependence of the order parameters on time, see Fig. 14. One observes periods of time, when two-clusters persist. These periods are characterized by almost constant order parameters. The periodic blowouts of the order parameters correspond to the behavior, during which the oscillators from the advancing cluster spread over a big part of the phase circle and finally form another cluster behind (see the inset in Fig. 14).

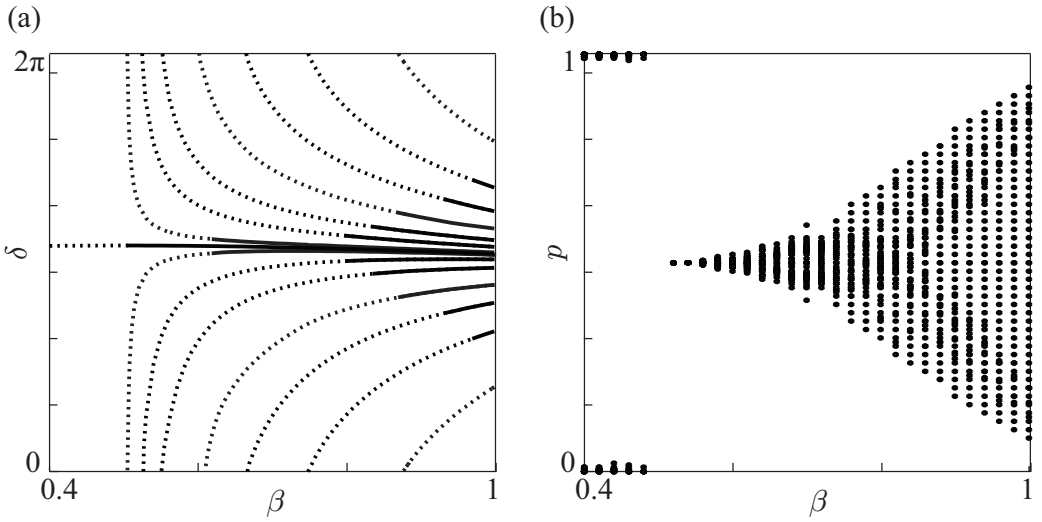

Figure 13: Stability and existence of two-cluster states. (a) Solid lines denote stable two-cluster stationary states and dashed - unstable. The lines are shown only for selected values of $p = N_1/N$, while the dense set of branches for all possible p exist. Figure (b) shows which two-clusters are stable in dependence on β (obtained numerically). $p = 0.5$ corresponds to the symmetric cluster and $p \neq 0.5$ to nonsymmetric clusters.

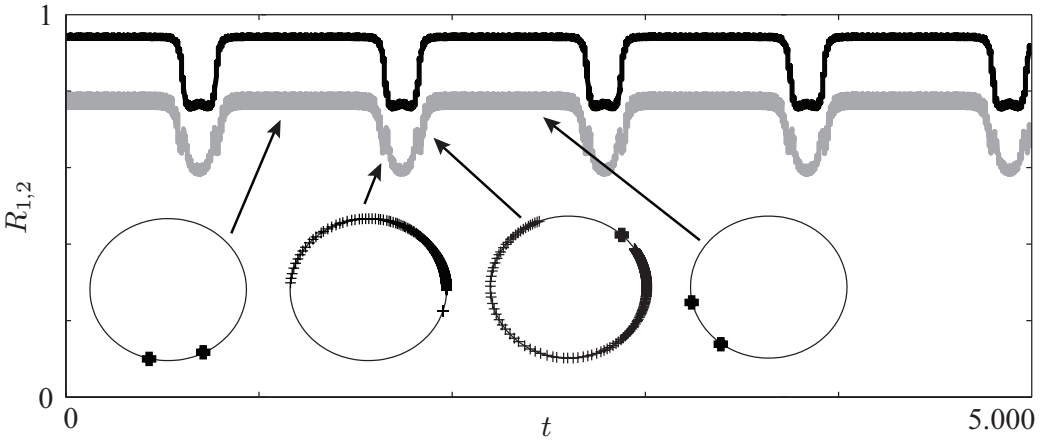

Figure 14: Nonstationary behavior of the order parameters R_1 and R_2 with time for $\beta = 0.5001$. One observes periodic restructuring of two-clusters.

6 Conclusions

In this paper we have studied the asymptotic behavior of a system of globally pulse-coupled phase oscillators (9)–(10) with the phase response function, which is positive, unimodal, and turns zero at the threshold together with its first derivative. In particular, we considered the question how the position of the maximum of the PRC influences the dynamics of the coupled system.

We have numerically observed, that for the PRCs with the maximum shifted to the right (for our model, it corresponds to $\beta < 0.5$), a one-cluster state becomes apparently stable. More detailed analysis reveals that the one-cluster state is, in fact, asymptotically locally unstable, i.e. a generic small perturbation will grow with time. Moreover, we show that trajectories of the system has a behavior, which is characterized by long-time intervals when the system stays close to the one-cluster state and long excursions away from the one-cluster state (see Fig. 10). The excursions become less and less frequent with time. This behavior is explained by the existence of the family of homoclinic orbits to the one-cluster state, which altogether form an attracting set in the phase space of the system.

In the case, when the maximum of the PRC is shifted to the left, i.e. the oscillators are mostly sensitive to perturbations in the phase just after the threshold, the one-cluster state no more dominates the dynamics and various stationary two-cluster states become stable. These two-cluster states appear in pitchfork bifurcations from the one-cluster state as parameter β increases. First, at $\beta = 0.5$, there appears a symmetric two-cluster with equal number of oscillators in each cluster. With further increasing β more and more asymmetric clusters appear and become stable leading to the increasing coexistence of stable two-clusters.

7 Appendix: Existence of a homoclinic orbit

Theorem. *For $\beta \in (0, 1)$ there exists N_0, such that for populations of size $N > N_0$, system (16) possesses a homoclinic trajectory, which connects the one-cluster stationary state. The homoclinic trajectory has the form*

$$2\pi = \varphi_2(n) = \cdots \varphi_N(n) \neq \varphi_1(n), \tag{35}$$

where $\lim_{n\to-\infty} \varphi_1(n) = 0^+$ and $\lim_{n\to+\infty} \varphi_1(n) = 2\pi^-$.

Proof. Fix $\beta \in (0,1)$. We will consider

$$Y_1(N,x) = 2\pi - \mu\left(N, 2\pi - \mu^{N-1}(N,x)\right),$$

where $\mu^j(N,x)$ denotes the j-th iteration of

$$x \mapsto \mu(N,x) = x + \frac{\varkappa}{N} Z_\beta(x).$$

The map $Y_1(N,x)$ describes the evolution of the distance $x \in (0,2\pi)$ during a time interval in which all oscillators of a population $\varphi_1 = x;\ \ \varphi_2 = ... = \varphi_N = 2\pi$, emit exactly one spike. Homoclinicity then is equivalent to

$$Y_1^k(N,x) \to 2\pi, \text{ for all } x \in (0,2\pi), \text{ as } k \to \infty,$$

where $Y_1^k(N,x)$ denotes the $k-th$ iteration of $x \mapsto Y_1(N,x)$. Analogously to the analysis of section 4, we find that

$$\begin{aligned} &Y_1(N,0) = 0; \quad Y_1(N,2\pi) = 2\pi, \\ &Y_1'(N,0) = Y_1'(N,2\pi) = 1, \\ &Y_1''(N,0) > 0, \quad Y_1''(N,2\pi) > 0. \end{aligned}$$

Here and in the following, primes denote the derivatives with respect to the second argument (phase). For fixed N, there exists a rejecting region $(0,\varepsilon_N)$ where $Y_1''(N,x) > 0$, for $x \in (0,\varepsilon_N)$ and an attracting region $(2\pi-\varepsilon_N, 2\pi)$ with $Y_1''(N,x) > 0$, for $x \in (2\pi-\varepsilon_N, 2\pi)$. This gives:

$$Y_1^{k_0}(N,x) > \varepsilon_N,$$

for $x \in (0,\varepsilon_N)$ and some finite $k_0 = k_0(N,x) \in \mathbb{N}$, and

$$Y_1^k(N,x) \to 2\pi,$$

for $k \to \infty$ and $x \in (2\pi-\varepsilon_N, 2\pi)$. Our goal is to show, that there exists a uniform $\varepsilon_0 > 0$, such that for all $N > N_0$:

$$\begin{aligned} &Y_1''(N,x) > 0 \quad \text{for } x \in (0,\varepsilon_0) \quad \text{and} \\ &Y_1''(N,x) > 0 \quad \text{for } x \in (\varepsilon_0, 2\pi-\varepsilon_0), \end{aligned}$$

and such that for all $N > N_0$ and all $x \in [\varepsilon_0, 2\pi-\varepsilon_0]$:

$$Y_1(N,x) > x + \Delta_N,$$

with

$$\Delta_N := \min_{x\in[\varepsilon_N, 2\pi-\varepsilon_N]} Y_1(N,x) - x > 0.$$

Thus, any $x \in (0, 2\pi)$ will reach the attracting region $(2\pi - \varepsilon_0, 2\pi)$ within a finite number of iterations of $x \mapsto Y_1(N,x)$. Let us write

$$Y_1(N,x) = \tilde{Y}_1(x) + \frac{1}{N} w(N,x),$$

where $\tilde{Y}_1(x) = x + \varkappa Z_\beta(x)$ is independent of N. For $\tilde{Y}_1$ we have

$$\begin{aligned} &\tilde{Y}_1(x) > x \quad \text{for } x \in (0, 2\pi), \\ &\tilde{Y}_1(0) = 0,\ \tilde{Y}_1(2\pi) = 2\pi, \\ &\tilde{Y}_1'(0) = \tilde{Y}_1'(2\pi) = 1, \end{aligned}$$

This implies for

$$w(N,x) = N\left(Y_1(N,x) - \tilde{Y}_1(x)\right),$$

that

$$\begin{aligned} &w(N,0) = w(N,2\pi) = 0, \\ &w'(N,0) = w'(N,2\pi) = 0. \end{aligned}$$

We will show, that the region $[0, \varepsilon_N]$ may be chosen as $[0, \varepsilon_0]$, independently on large N. The analysis for the other region $[2\pi - \varepsilon_0, 2\pi]$ can be done similarly. Around $x = 0$, we have the following representation of $Y_1(N,x)$:

$$Y_1(N,x) = Y_1(N,0) + Y_1'(N,0)\,x + \frac{x^2}{2} Y_1''(N,\xi_N)$$

$$= \tilde{Y}_1(0) + \tilde{Y}_1'(0)\,x + \frac{x^2}{2}\tilde{Y}_1''(\xi_N) + \frac{1}{N}\left(w(N,0) + w'(N,0)\,x + \frac{x^2}{2} w''(N,\xi_N)\right)$$

$$= x + \frac{x^2}{2}\left(\tilde{Y}_1''(\xi_N) + \frac{1}{N} w''(N,\xi_N)\right)$$

for some $\xi_N \in [0, \varepsilon]$. Further it holds $\tilde{Y}_1''(0) > 0$. This means, there exists an $\varepsilon_0 > 0$, such that for $x \in [0, \varepsilon_0]$, $\tilde{Y}_1''(x) > 0$. Now we construct an N-independent lower bound for $w''(N,x)$ in $x \in [0, \varepsilon_0]$, where ε_0 will be further

altered in the analysis without always choosing a new notation. In other words, we claim that there exists $c_0 \in \mathbb{R}$ with

$$\liminf_{N\to\infty}\left(\min_{x\in[0,\varepsilon_0]} w''(N,x)\right) > c_0. \tag{36}$$

We have

$$\begin{aligned}
w(N,\varepsilon) &= N\left(Y_1(N,x) - \tilde{Y}_1(x)\right)\\
&= N\left(2\pi - \mu\left(2\pi - \mu^{N-1}(N,x)\right) - x - \varkappa Z_\beta(x)\right)\\
&= N\left(\mu^{N-1}(N,x) - \frac{\varkappa}{N} Z_\beta\left(2\pi - \mu^{N-1}(N,x)\right) - x - \varkappa Z_\beta(x)\right)\\
&= N\left(\frac{\varkappa}{N}\sum_{j=0}^{N-2} Z_\beta\left(\mu^j(N,x)\right) - \frac{\varkappa}{N} Z_\beta\left(2\pi - \mu^{N-1}(N,x)\right) - \varkappa Z_\beta(x)\right)\\
&= \varkappa\sum_{j=0}^{N-2}\left(Z_\beta\left(\mu^j(N,x)\right) - Z_\beta(x)\right) - \underbrace{\varkappa Z_\beta\left(2\pi - \mu^{N-1}(N,x)\right) - \varkappa Z_\beta(x)}_{\equiv \mathrm{I}}.
\end{aligned}$$

Since part I, as well as its derivatives, is obviously uniformly bounded in N and x, we restrict us to establish (36) for

$$\tilde{w}(N,x) = \sum_{j=0}^{N-2}\left[Z_\beta\left(\mu^j(N,x)\right) - Z_\beta(x)\right].$$

We have

$$\tilde{w}'(N,x) = \sum_{j=0}^{N-2}\left[Z'_\beta\left(\mu^j(N,x)\right)\left(\mu^j(N,x)\right)' - Z'_\beta(x)\right],$$

$$\begin{aligned}
\tilde{w}''(N,x) &= \sum_{j=0}^{N-2}\Big[Z''_\beta\left(\mu^j(N,x)\right)\left(\left(\mu^j(N,x)\right)'\right)^2 \\
&\quad + Z'_\beta\left(\mu^j(N,x)\right)\left(\mu^j(N,x)\right)'' - Z''_\beta(x)\Big].
\end{aligned} \tag{37}$$

To handle this, we need some uniformity-properties of $\mu^j(N,x)$. Elementary calculations give

$$\left(\mu^j(N,x)\right)' = \prod_{k=0}^{j-1}\mu'\left(N,\mu^k(N,x)\right) = \prod_{k=0}^{j-1}\left(1 + \frac{\varkappa}{N} Z'_\beta\left(\mu^k(N,x)\right)\right),$$

$$\left(\mu^j(N,x)\right)'' = \sum_{l=0}^{j} \prod_{k=0,\,k\neq l}^{j-1} \left[\left(1+\frac{\varkappa}{N} Z_\beta'\left(\mu^k(N,x)\right)\right)\right] \times \frac{\varkappa}{N} Z_\beta''\left(\mu^l(N,x)\right)\left(\mu^l(N,x)\right)'.$$

This implies that the following inequality

$$0 < \left(\mu^j(N,x)\right)' < \exp(\varkappa\zeta'), \quad \text{where} \quad \zeta' \equiv \max_{x\in[0,2\pi]} \left|Z_\beta'(x)\right| \tag{38}$$

holds for all large enough N. This again yields

$$\begin{aligned} x \le \mu^j(N,x) &= \mu^j(N,0) + \int_0^x \left(\mu^j(N,y)\right)' dy \\ &\le x + x\exp(\varkappa\zeta'). \end{aligned} \tag{39}$$

Using this upper bound, we get some N-independent ε_0, such that for $x \in [0,\varepsilon_0]$

$$Z_\beta''\left(\mu^k(N,x)\right) > 0.$$

This gives N-independent monotonicity of

$$x \mapsto Z_\beta'\left(\mu^k(N,x)\right) > 0 \quad \text{for} \quad x \in (0,\varepsilon_0).$$

Further, we can use (39) to improve the bounds (38) for $\left(\mu^j(N,x)\right)'$ in $x \in [0,\varepsilon_0]$ to

$$1 \le \left(\mu^j(N,x)\right)' < \exp(\varkappa\zeta'). \tag{40}$$

This implies

$$\mu^j(N,x) < x\cdot\exp(\varkappa\zeta').$$

We find

$$0 < \left(\mu^j(N,x)\right)'' \le \frac{j\varkappa\zeta''}{N}\exp(2\varkappa\zeta') \le \varkappa\zeta''\exp(2\varkappa\zeta'),$$

where

$$\zeta'' \equiv \max_{x\in[0,2\pi]} \left|Z_\beta''(x)\right|.$$

Now observe that

$$Z_\beta''(0) + Z_\beta'''(0) = \left(4-\frac{8}{\pi}\right)\beta^2 + \frac{2}{\pi}\beta + \frac{1}{\pi} > 0,$$

i.e., eventually further decreasing of $\varepsilon_0 > 0$ gives, with $\tilde{\varepsilon}_0 = \varepsilon_0 \cdot \exp(\varkappa\zeta')$:

$$\min_{y\in[0,\tilde{\varepsilon}_0]} Z''_\beta(y) > -\min_{y\in[0,\tilde{\varepsilon}_0]} Z'''_\beta(y). \tag{41}$$

Hence, for $x \in [0, \varepsilon_0]$:

$$\begin{aligned}
\tilde{w}''(N,x) &= \sum_{j=0}^{N-2}\left(Z''_\beta\left(\mu^j\right)\left(\left(\mu^j\right)'\right)^2 + \underbrace{Z'_\beta\left(\mu^j\right)\left(\mu^j\right)''}_{\geq 0} - Z''_\beta(x)\right)\\
&\geq \sum_{j=0}^{N-2}\left(Z''_\beta\left(\mu^j\right)\left(\left(\mu^j\right)'\right)^2 - Z''_\beta\left(\mu^j\right) + \int_x^{\mu^j} Z'''_\beta(y)\,dy\right)\\
&= \sum_{j=0}^{N-2}\left(Z''_\beta\left(\mu^j\right)\left(\left(\left(\mu^j\right)'\right)^2 - 1\right) + \int_x^{\mu^j} Z'''_\beta(y)\,dy\right)\\
&\geq \sum_{j=0}^{N-2}\left(\min_{y\in[0,\tilde{\varepsilon}_0]} Z''_\beta(y)\left(\left(\left(\mu^j\right)'\right)^2 - 1\right) + \min_{y\in[0,\tilde{\varepsilon}_0]} Z'''_\beta(y)\left(\mu^j - x\right)\right),
\end{aligned}$$

where we have omitted the arguments (N, x) of μ for brevity. Using (41), we continue the estimations

$$\begin{aligned}
\cdots &\geq \sum_{j=0}^{N-2}\left(\min_{y\in[0,\tilde{\varepsilon}_0]} Z''_\beta(y)\left(\left(\left(\mu^j\right)'\right)^2 - 1 - \left(\mu^j - x\right)\right)\right)\\
&= \min_{y\in[0,\tilde{\varepsilon}_0]} Z''_\beta(y)\sum_{j=0}^{N-2}\left(\left(\underbrace{\left(\mu^j\right)'}_{\geq 1}\right)^2 - 1 - \int_0^x\left(\underbrace{\left(\mu^j\right)'}_{\leq \mu^j} - 1\right)dy\right)\\
&\geq \min_{y\in[0,\tilde{\varepsilon}_0]} Z''_\beta(y)\sum_{j=0}^{N-2}\left(\left(\left(\mu^j\right)'\right) - 1 - x\left(\left(\mu^j\right)' - 1\right)\right)\\
&\geq \min_{y\in[0,\tilde{\varepsilon}_0]} Z''_\beta(y)\sum_{j=0}^{N-2}(1-x)\left(\left(\mu^j\right)' - 1\right) \geq 0.
\end{aligned}$$

This establishes (36) and hence $Y_1(N,x) > x \in [0,\varepsilon_0]$ for large enough N. $\square$

References

[1] Pikovsky, A., Rosenblum, M., and Kurths, J. (2001) *Synchronization. A Universal Concept in Nonlinear Sciences*, Cambridge University Press.

[2] Strogatz, S.H. (2001) Exploring complex networks. *Nature*, **410**, 268 – 276.

[3] Strogatz, S.H., Abrams, D.M., McRobie, A., Eckhardt, B., and Ott, E. (2005) Theoretical mechanics: Crowd synchrony on the millennium bridge. *Nature*, **438** (7064), 43–44.

[4] Tass, P. (1999) *Phase Resetting in Medicine and Biology. Stochastic Modelling and Data Analysis*, Springer Series in Synergetics, Springer.

[5] Timme, M., Geisel, T., and Wolf, F. (2006) Speed of synchronization in complex networks of neural oscillators: Analytic results based on random matrix theory. *Chaos*, **16**, 015 108.

[6] Popovych, O.V., Hauptmann, C., and Tass, P.A. (2006) Control of neuronal synchrony by nonlinear delayed feedback. *Biol Cybern*, **95** (1), 69–85.

[7] Wünsche, H.J., Bauer, S., Kreissl, J., Ushakov, O., Korneyev, N., Henneberger, F., Wille, E., Erzgräber, H., Peil, M., Elsäßer, W., and Fischer, I. (2005) Synchronization of delay-coupled oscillators: A study of semiconductor lasers. *Phys. Rev. Lett.*, **94**, 163 901–1–163 901–4.

[8] Fischer, I., Vicente, R., Buldú, J.M., Peil, M., Mirasso, C.R., Torrent, M.C., and Garcia-Ojalvo, J. (2006) Zero-lag long-range synchronization via dynamical relaying. *Phys. Rev. Lett.*, **97**, 123902.

[9] Yanchuk, S., Schneider, K.R., and Recke, L. (2004) Dynamics of two mutually coupled semiconductor lasers: Instantaneous coupling limit. *Phys. Rev. E*, **69**, 056 221–1–056 221–12.

[10] Yanchuk, S., Stefanski, A., Kapitaniak, T., and Wojewoda, J. (2006) Dynamics of an array of coupled semiconductor lasers. *Phys. Rev. E*, **73**, 016209.

[11] Cuomo, K.M. and Oppenheim, A.V. (1993) Circuit implementation of synchronized chaos with applications to communications. *Phys. Rev. Lett.*, **71** (1), 65–68, doi:10.1103/PhysRevLett.71.65.

[12] Kanter, I., Kopelowitz, E., and Kinzel, W. (2008) Public channel cryptography: Chaos synchronization and hilbert's tenth problem. *Phys. Rev. Lett.*, **101** (8), 084 102.

[13] Perlikowski, P., Stefanski, A., and Kapitaniak, T. (2008) 1:1 mode locking and generalized synchronization in mechanical oscillators. *Journal of Sound and Vibration*, **318** (1-2), 329 – 340.

[14] Perlikowski, P., Yanchuk, S., Wolfrum, M., Stefanski, A., Mosiolek, P., and Kapitaniak, T. (2010) Routes to complex dynamics in a ring of unidirectionally coupled systems. *Chaos*, **20**, 013 111.

[15] Elble, R. and Koller, W. (1990) *Tremor*, The John Hopkins University Press.

[16] Mirollo, R. and Strogatz, S. (1990) Synchronization of pulse-coupled biological oscillators. *SIAM J. Appl. Math.*, **50** (6), 1645–1662.

[17] Bottani, S. (1996) Synchronization of integrate and fire oscillators with global coupling. *Phys. Rev. E*, **54** (3), 2334–2350.

[18] Tsodyks, M., Mitkov, I., and Sompolinsky, H. (1993) Pattern of synchrony in inhomogeneous networks of oscillators with pulse interactions. *Phys. Rev. Lett.*, **71** (8), 1280–1283.

[19] Goel, P. and Ermentrout, B. (2002) Synchrony, stability, and firing patterns in pulse-coupled oscillators. *Physica D: Nonlinear Phenomena*, **163** (3-4), 191 – 216.

[20] LaMar, M.D. and Smith, G.D. (2010) Effect of node-degree correlation on synchronization of identical pulse-coupled oscillators. *Phys. Rev. E*, **81** (4), 046 206.

[21] Guardiola, X., Díaz-Guilera, A., Llas, M., and Pérez, C.J. (2000) Synchronization, diversity, and topology of networks of integrate and fire oscillators. *Phys. Rev. E*, **62** (4), 5565–5570.

[22] Bressloff, P.C., Coombes, S., and de Souza, B. (1997) Dynamics of a ring of pulse-coupled oscillators: Group-theoretic approach. *Phys. Rev. Lett.*, **79** (15), 2791–2794.

[23] Ernst, U., Pawelzik, K., and Geisel, T. (1995) Synchronization induced by temporal delays in pulse-coupled oscillators. *Phys. Rev. Lett.*, **74** (9), 1570–1573.

[24] Zumdieck, A., Timme, M., Geisel, T., and Wolf, F. (2004) Long chaotic transients in complex networks. *Phys. Rev. Lett.*, **93** (24), 244 103.

[25] Zillmer, R., Livi, R., Politi, A., and Torcini, A. (2007) Stability of the splay state in pulse-coupled networks. *Phys. Rev. E*, **76** (4), 046102.

[26] Abbott, L.F. and van Vreeswijk, C. (1993) Asynchronous states in networks of pulse-coupled oscillators. *Phys. Rev. E*, **48** (2), 1483–1490.

[27] Olmi, S., Livi, R., Politi, A., and Torcini, A. (2010) Collective oscillations in disordered neural networks. *Phys. Rev. E*, **81** (4), 046 119.

[28] Brown, E., Moehlis, J., and Holmes, P. (2004) On the phase reduction and response dynamics of neural oscillator populations. *Neural Computation*, **16**, 673?715.

[29] Izhikevich, E.M. (2005) *Dynamical Systems in Neuroscience: The Geometry of Excitability and Bursting*, The MIT Press.

[30] Hoppensteadt, F. and Izhikevich, E. (1997) *Weakly Connected Neural Networks*, Springer-Verlag, New York.

[31] Ermentrout, B. (1996) Type i membranes, phase resetting curves, and synchrony. *Neural Computation*, **8** (5), 979–1001.

[32] Tass, P. A. (2003) A model of desynchronizing deep brain stimulation with a demand-controlled coordinated reset of neural subpopulations, *Biological cybernetics*, **89** (2), 81-88